JOURNAL OF SOLID STATE CHEMISTRY 114, 151–158 (1995)

Two New Adamite-Type Phases, $Co_2(OH)PO_4$ and $Zn_2(OH)PO_4$: Structure-Directing Effect of Organic Additives

William T. A. Harrison,* J. T. Vaughey,* Laurie L. Dussack,* Allan J. Jacobson,* Theresa E. Martin,†[1] and Galen D. Stucky†

*Department of Chemistry, University of Houston, Houston, Texas 77204-5641; and †Department of Chemistry, University of California, Santa Barbara, California 93106-9510

Received February 10, 1994; accepted April 21, 1994

The hydrothermal syntheses, X-ray single crystal structures, and certain properties of cobalt hydroxyphosphate, $Co_2(OH)PO_4$, and zinc hydroxyphosphate, $Zn_2(OH)PO_4$, are described. Both materials are isomorphous with the adamite-type $M_2(OH)XO_4$ structure, and consist of a condensed vertex- and edge-sharing network of MO_5, distorted MO_6 (M = Co, Zn), and PO_4 subunits. Both snythetic procedures required the presence of organic reagents which are not incorporated into the crystalline reaction products. Crystal data: $Co_2(OH)PO_4$, $M_r = 229.84$, orthorhombic, space group *Pnnm* (No. 58), $a = 8.042(3)$ Å, $b = 8.369(2)$ Å, $c = 5.940(2)$ Å, $V = 399.80$ Å^3, $Z = 4$, $R = 2.40\%$, and $R_w = 2.71\%$ (589 observed reflections with $I > 3\sigma(I)$). $Zn_2(OH)PO_4$, $M_r = 242.74$, orthorhombic, space group *Pnnm* (No. 58), $a = 8.103(2)$, Å, $b = 8.3292(9)$ Å, $c = 5.9659(8)$ Å, $V = 402.65$ Å^3, $Z = 4$, $R = 3.58\%$, and $R_w = 3.90\%$ (708 data with $I > 3\sigma(I)$).

INTRODUCTION

The complex structural chemistry of minerals of the formula $ABXO_4(Z)$ has been recognized for many years (1), and several structural types have been elucidated for this general formula. The adamite-type $M_2(O/OH)XO_4$ family of phases includes such naturally occurring materials as $Zn_2(OH)AsO_4$ (adamite) (2), $Mn_2(OH)AsO_4$ (eveite) (3), $Cu_2(OH)PO_4$ (libethenite) (4), $Cu_2(OH)AsO_4$ (olivenite) (5), $Co_2(OH)AsO_4$ (6), Al_2OSiO_4 (andalusite) (7), and $Al_{1.14}Mn_{0.86}OSiO_4$ (kanonaite) (8). Some recently prepared synthetic analogues, in the solid solution $Fe_{2-x}Al_xOGeO_4$ (9), also crystallize in the adamite-type structure. All these phases contain a condensed network of vertex- and edge-sharing MO_5, MO_6, and XO_4 subunits, and crystallize in an orthorhombic cell (space group *Pnnm*).

In this paper, we report the preparations, crystal structures, and certain properties of two new synthetic adamite-type phases, $Co_2(OH)PO_4$ and $Zn_2(OH)PO_4$. Both hydrothermal syntheses require the presence of organic additives which are not incorporated into the final product.

[1] Present address: Central Research Division, Dow Corning Corporation, Midland, Michigan 48640.

SYNTHESIS AND INITIAL CHARACTERIZATION

Dark-purple prismatic rods (maximum linear dimension ~1.0 mm) of $Co_2(OH)PO_4$ were prepared in >95% yield, with respect to cobalt, from a reaction mixture of initial composition 0.60 g $Co(NO_3)_2 \cdot H_2O$ (99.999%, Aldrich), 1.0 ml H_3PO_4 (85%, Fisher), 6 ml dimethylamine (DMA) (40% in water, Aldrich), 1.0 g 1,4-diazabicyclo[2.2.2]octane (DABCO) (98%, Aldrich), and 10 ml of distilled water. The pH of the mixture was lowered to 8.0 by the dropwise addition of a dilute hydrochloric acid solution; the mixture was then heated to 200°C for 4 days in a sealed, 23-ml Teflon-lined Parr hydrothermal bomb. The bomb was slowly cooled to room temperature over 2 days, and a large mass of air-stable purple crystals was recovered by vacuum filtration.

Reducing the pH to ~2.2 for similar reactions resulted in the isolation of chunky single crystals of the known cobalt (hydrogen)phosphate $Co_7(HPO_4)_4(PO_4)_3$ (10), while reactions in the intermediate pH range between 2.2 and 8.0 yielded pale purple powders of unknown composition, but no single crystals. Further $Co/PO_4/OH/H_2O$ syntheses at ~pH 8, in which NH_4OH was used to raise the pH, but which excluded the organic additives, resulted in purple powders with completely different X-ray powder patterns from that of adamite-type $Co_2(OH)PO_4$. A preliminary analysis indicated the presence of $NH_4CoPO_4 \cdot H_2O$ (11) and other phase(s). These materials are being studied further and will be described later.

Translucent, irregular, single crystals (up to ~0.75 mm in size) of $Zn_2(OH)PO_4$ were prepared from a mixture comprising 11.35 g 40% tetraethylammonium hydroxide (TEA) (0.0305 mol), 1.052 g $ZnCl_2$ (0.0077 mol), 1.486 g 85.4% H_3PO_4 (0.0127 mol), and 5 ml water (0.277 mol),

0022-4596/95 $6.00

which resulted in a thick, white gel that partially dissolved upon standing. The mixture was sealed in a Teflon-lined hydrothermal Parr bomb, and heated to 150°C for 4 days. Upon recovery from the pH 8 mother liquor by vacuum filtration and after being washed with water, 0.86 g of solid material was recovered. A portion of this product was sonicated in a 50/50 acetone/water mixture, and the differently sized particles were separated by washing over 80 and 170-mesh microsieves. Beads of pure (as determined by powder X-ray) $Zn_2(OH)PO_4$ adamite were recovered from the 170-mesh screen and used for the X-ray TGA, and IR analyses described below. $Zn_2(OH)PO_4$ crystals are indefinitely stable in air. The fines which passed through the 170-mesh screen comprised adamite-type $Zn_2(OH)PO_4$ and other, unidentified phases.

Similar zinc/phosphate/TEA reactions were carried out at varying pH's, attained by altering the concentration of the organic base. Reactions in the pH range 3.5–7.6, and at pH 10.0 led to single crystals and powders of hopeite, $Zn_3(PO_4)_2 \cdot 4H_2O$ (12), and other unidentified phases (powder X-ray diffraction). Thus, the pH range for the formation of $Zn_2(OH)PO_4$ appears to be a narrow one (~8.0–8.5); hopeite forms if the pH is too low *or* too high. Reactions which substituted ammonium hydroxide from the organic base led to the known phase NH_4ZnPO_4 (13) in the pH 6–10 range.

X-ray powder data for thoroughly ground samples of $Co_2(OH)PO_4$ and $Zn_2(OH)PO_4$ were collected on a Scintag XDS 2000 automated diffractometer (θ–θ geometry, flat plate sample, Cu$K\alpha$ radiation, $\bar{\lambda} = 1.54178$ Å, $T = 25(2)$°C). The instrumental $K\alpha_1/K\alpha_2$ profile was reduced to a single Cu$K\alpha_1$ peak ($\lambda = 1.540568$ Å) by a software "stripping" routine, and d-spacings were located relative to this wavelength. Prior to least-squares minimization of the lattice parameters, index-to-peak assignments were made on the basis of LAZY-PULVERIX (14) simulations using the single-crystal parameters described below. Refined values of $a = 8.043(2)$ Å, $b = 8.376(2)$ Å, and $c = 5.951(1)$ Å ($V = 400.9(2)$ Å^3) were obtained for $Co_2(OH)PO_4$. Values of $a = 8.088(2)$ Å, $b = 8.313(2)$ Å, and $c = 5.9575(9)$ Å ($V = 400.6(2)$ Å^3) resulted for the $Zn_2(OH)PO_4$ refinement. The powder patterns of $Co_2(OH)PO_4$ and $Zn_2(OH)PO_4$ are listed in Tables 1 and 2, respectively.

Thermogravimetric analysis (TGA) data for $Co_2(OH)PO_4$ were collected on a computer-controlled DuPont 2100 system, with a heating rate of 5°C/min, in air. Infrared (IR) data for $Co_2(OH)PO_4$ were collected on a Galaxy FTIR 5000 Series spectrometer (KBr pellet). TGA and IR data for $Zn_2(OH)PO_4$ were collected in a similar fashion.

TABLE 1
X-Ray Powder Data for $Co_2(OH)PO_4$

h	k	l	d_{obs}	d_{calc}	Δd^a	$I_{rel}{}^b$
1	1	0	5.800	5.801	−0.002	100
0	1	1	4.848	4.851	−0.003	33
1	0	1	4.783	4.784	−0.001	39
1	1	1	4.154	4.154	0.000	6
1	2	0	3.715	3.714	0.001	23
2	1	0	3.625	3.625	0.000	26
0	0	2	2.976	2.976	0.000	9
2	2	0	2.900	2.901	0.000	94
1	1	2	2.649	2.648	0.001	46
2	2	1	2.608	2.607	0.001	13
3	1	0	2.553	2.553	0.000	21
0	3	1	2.528	2.528	0.000	4
3	0	1	2.444	2.444	0.000	13
0	2	2	2.426	2.426	0.000	12
1	3	1	2.412	2.411	0.001	13
2	0	2	2.392	2.392	0.000	5
3	1	1	2.347	2.347	0.000	8
2	1	2	2.299	2.300	−0.001	39
3	2	0	2.257	2.258	−0.001	6
2	2	2	2.077	2.077	0.000	6
1	3	2	1.974	1.974	0.000	3
1	4	1	1.919	1.918	0.001	8
4	1	1	1.858	1.858	0.000	6
2	3	2	1.817	1.816	0.000	2
4	0	2	1.666	1.666	0.000	7
1	5	0	1.640	1.640	0.000	2
3	3	2	1.621	1.621	0.000	6
3	0	3	1.595	1.595	0.000	3
3	4	1	1.590	1.590	0.000	3
1	3	3	1.585	1.585	0.000	2
1	5	1	1.580	1.581	−0.001	3
2	4	2	1.575	1.576	0.000	7
4	2	2	1.548	1.548	0.000	5

[a] $d_{obs} - d_{calc}$.
[b] $100 \times I/I_{max}$.

CRYSTAL STRUCTURE DETERMINATION

The structures of $Co_2(OH)PO_4$ and $Zn_2(OH)PO_4$ were determined by standard single-crystal X-ray methods. For each phase, a suitable single crystal was mounted on a thin glass fiber with cyanoacrylate adhesive, prior to data collection. For $Co_2(OH)PO_4$, a purple rod of dimensions ~0.4 × 0.05 × 0.05 mm was used; for $Zn_2(OH)PO_4$, a transparent, irregular chunk, with dimensions ~0.3 × 0.4 × 0.4 mm, was chosen. During preliminary X-ray measurements, instrumental-resolution peak scans (ω-scan width < 0.2°) were observed for both compounds.

Room-temperature (25(2)°C) intensity data for $Co_2(OH)PO_4$ were collected on an Enraf–Nonius automated 4-circle diffractometer (graphite-monochromated Mo$K\alpha$ radiation, $\lambda = 0.71073$ Å). Twenty-five reflections ($7° < 2\theta < 19°$) were located and centered by searching reciprocal space and were indexed to obtain a unit cell and orientation matrix; the unit cell constants were optimized by a least-squares refinement, resulting in lattice parameters of $a = 8.042(3)$ Å, $b = 8.369(2)$ Å, and

TABLE 2
X-Ray Powder Data for $Zn_2(OH)PO_4$

h	k	l	d_{obs}	d_{calc}	Δd^a	I_{rel}^b
1	1	0	5.795	5.797	−0.002	50
0	1	1	4.840	4.842	−0.002	50
1	0	1	4.794	4.797	−0.003	100
0	2	0	4.154	4.156	−0.002	2
1	2	0	3.696	3.697	−0.001	21
2	1	0	3.637	3.637	0.000	37
0	0	2	2.978	2.979	0.000	16
2	2	0	2.899	2.898	0.000	59
1	1	2	2.650	2.649	0.000	96
1	3	0	2.622	2.621	0.001	30
2	2	1	2.607	2.606	0.001	20
3	1	0	2.565	2.565	0.000	44
0	3	1	2.513	2.512	0.001	16
3	0	1	2.457	2.456	0.000	23
0	2	2	2.421	2.421	0.000	43
2	0	2	2.399	2.398	0.001	44
3	1	1	2.356	2.356	0.000	24
2	1	2	2.305	2.304	0.000	43
2	2	2	2.078	2.077	0.000	11
1	3	2	1.968	1.968	0.001	6
0	1	3	1.931	1.931	0.000	13
4	1	1	1.866	1.866	0.000	11
0	4	2	1.704	1.704	0.000	13
3	3	2	1.621	1.621	0.000	23
3	0	3	1.599	1.599	0.000	6
3	4	1	1.587	1.587	0.000	11
2	4	2	1.570	1.571	0.000	23
4	2	2	1.552	1.552	0.000	10

[a] $d_{obs} - d_{calc}$.
[b] $100 \times I/I_{max}$.

c = 5.940(2) Å. Intensity data were collected in the ω–2θ scanning mode with standard reflections monitored for intensity variation throughout the course of each experiment: < ±2% variation was recorded. The scanning speed varied from 0.7 to 3.4°/min, with a scanning range of $(1.0 + 0.35 \tan \theta)°$. During data reduction, crystal absorption was corrected for on the basis of ψ-scans through 360° for selected reflections with $\chi \approx 90°$ (min = 1.00, max = 1.40).

The $Co_2(OH)PO_4$ raw data were reduced to F^2 and $\sigma(F^2)$ values with the program RC85(15): the systematic absences ($h0l$, $h + l$; $0kl$, $k + l$) indicated space groups $Pnn2$ (No. 34) or $Pnnm$ (No. 58). After successful structure solution in $Pnnm$, the centrosymmetric space group was assumed in all subsequent calculations.

For $Zn_2(OH)PO_4$, room-temperature (25(2)°C) intensity data were collected on a Huber automated 4-circle diffractometer (graphite-monochromated Mo$K\alpha$ radiation, λ = 0.71073 Å). Twenty reflections were located and centered in reciprocal space and indexed to obtain a unit cell (least-squares optimized values: a = 8.103(2) Å, b = 8.3292(9) Å, c = 5.9659(8) Å) and an orientation matrix. Intensity data were collected in the θ–2θ scanning mode with standard reflections monitored for intensity variation throughout the course of the experiment (negligible variation was observed). The scanning speed was 6°/min with a scanning range of 1.3° below $K\alpha_1$ to 1.6° above $K\alpha_2$. Crystal absorption was corrected for on the basis of ψ-scans through 360° for selected reflections with $\chi \approx 90°$ (min = 1.0, max = 1.49).

The $Zn_2(OH)PO_4$ raw data were reduced using a Lehmann–Larsen profile-fitting routine (16), and the normal corrections for Lorentz and polarization effects were made. Systematic absences ($h0l$, $h + l$; $0kl$, $k + l$) indicated space groups $Pnn2$ or $Pnnm$. The structure was successfully developed in $Pnnm$, which was assumed in all subsequent analysis.

Both crystal structures were partially solved by using the direct-methods program SHELXS-86 (17); the other atom positions were located from Fourier difference maps during the refinement procedure. At this stage, it became apparent that both $Co_2(OH)PO_4$ and $Zn_2(OH)PO_4$ were isomorphs of the $M_2(OH)XO_4$ adamite-type structure (*vide infra*), and for ease of comparison with related structures, the atom coordinates for $Co_2(OH)PO_4$ and $Zn_2(OH)PO_4$ were reset to conform to the equivalent atom positions in $Zn_2(OH)AsO_4$, as reported by Hawthorne (2). The final full-matrix least-squares refinements for $Co_2(OH)PO_4$ and $Zn_2(OH)PO_4$ were against F and included anisotropic temperature factors for the nonhydrogen atoms, and a Larson-type secondary extinction correction (18). Complex, neutral-atom scattering factors were obtained from the "International Tables" (19). For both structures, a bond-distance restraint (d(O–H) = 0.95(1) Å) was used to stabilize the refinement of the hydrogen-atom position. At the end of the refinements, analysis of the various trends in F_o versus F_c revealed no unusual effects. The least-squares, Fourier, and subsidiary calculations were performed using the Oxford CRYSTALS system (20) on a DEC MicroVAX 3100 computer. Supplementary tables of anisotropic thermal factors and observed and calculated structure factors are available directly from the authors. Final residuals of R = 2.40% and R_w = 2.71% (Tukey–Prince weighting scheme (21) with Chebychev coefficients 2.3(2), −0.9(2), and 1.7(2)) were obtained for $Co_2(OH)PO_4$. The corresponding values for $Zn_2(OH)PO_4$ were R = 3.58% and R_w = 3.90% (coefficients 5.8(7), 0.7(6) and 2.1(7)). Crystallographic data for both phases are summarized in Table 3.

CRYSTAL STRUCTURES OF $Co_2(OH)PO_4$ AND $Zn_2(OH)PO_4$

Refined atomic positional and thermal parameters for $Co_2(OH)PO_4$ are listed in Table 4, with selected geometrical data in Table 5. Similar data for $Zn_2(OH)PO_4$ are presented in Tables 6 and 7, respectively. Both $Co_2(OH)PO_4$

TABLE 3
Crystallographic Parameters

	$Co_2(OH)PO_4$	$Zn_2(OH)PO_4$
Empirical formula	Co_2PO_5H	Zn_2PO_5H
Formula wt.	229.84	242.74
Habit	Purple rod	Colorless lump
Crystal system	Orthorhombic	Orthorhombic
a (Å)	8.042(3)	8.103(2)
b (Å)	8.369(3)	8.3292(9)
c (Å)	5.940(2)	5.9659(8)
V (Å^3)	399.80	402.65
Z	4	4
Space group	*Pnnm* (No. 58)	*Pnnm* (No. 58)
T (°C)	25(2)	25(2)
λ(Mo$K\alpha$) (Å)	0.71073	0.71073
ρ_{calc} (g/cm^3)	3.82	4.00
μ(Mo$K\alpha$) (cm^{-1})	85.90	125.15
Absorption corr.	ψ-scan	ψ-scan
Extinction corr.	8(1)	17(2)
hkl data limits	0 → 12, 0 → 12, 0 → 8	0 → 12, 0 → 12, 0 → 8
Total data	861	1247
Observed data[a]	589	708
Parameters	49	49
min, max $\Delta\rho$ (eÅ^{-3})	−0.6, +0.6	−0.2, +1.3
$R(F)$[b] (%)	2.40	3.58
$R_w(F)$[c] (%)	2.71	3.90

[a] $I > 3\sigma(I)$ after merging.
[b] $R = \Sigma \big| |F_o| - |F_c| \big| / \Sigma |F_o|$.
[c] $R_w = [\Sigma w(|F_o| - |F_c|)^2 / \Sigma w|F_o|^2]^{1/2}$, with weights as described in the text.

and $Zn_2(OH)PO_4$ are isostructural with adamite, $Zn_2(OH)AsO_4$ (2), and the other phases mentioned in the Introduction, and the description of the $Co_2(OH)PO_4$ and $Zn_2(OH)PO_4$ structures given below supplements those given earlier (2–7).

The asymmetric unit and complete crystal structure of $Co_2(OH)PO_4$ are illustrated in Figs. 1 and 2 respectively.

TABLE 4
Atomic Positional and Thermal Parameters for $Co_2(OH)PO_4$

Atom	x	y	z	U_{eq}[a]
Co(1)	0.36187(8)	0.36588(7)	1/2	0.0076
Co(2)	1/2	0	0.2548(1)	0.0079
P(1)	0.2476(1)	0.2405(1)	0	0.0060
O(1)	0.1094(4)	0.1124(4)	0	0.0102
O(2)	0.4137(4)	0.1484(4)	0	0.0078
O(3)	0.2315(3)	0.3481(3)	0.2092(4)	0.0090
O(4)	0.3829(4)	0.1234(4)	1/2	0.0082
H(1)	0.274(2)	0.080(5)	1/2	0.03(2)[b]

[a] U_{eq}(Å^2) = $(U_1U_2U_3)^{1/3}$.
[b] U_{iso} (Å^2).

TABLE 5
Distances (Å) and Angles (°) for $Co_2(OH)PO_4$

Co(1)–O(1)	2.076(3)	Co(1)–O(1)′	1.999(3)
Co(1)–O(3) × 2	2.026(2)	Co(1)–O(4)	2.036(3)
Co(2)–O(2) × 2	2.077(2)	Co(2)–O(3) × 2	2.264(2)
Co(2)–O(4) × 2	2.019(2)		
P(1)–O(1)	1.544(3)	P(1)–O(2)	1.542(3)
P(1)–O(3) × 2	1.541(2)		
O(3) ··· H(1)[a]	2.30(3)	O(4)–H(1)	0.95(1)
O(1)–Co(1)–O(1)′	78.4(1)	O(3)–Co(1)–O(1)	97.49(8)
O(3)–Co(1)–O(1)	121.47(7)	O(3)–Co(1)–O(3)	117.0(1)
O(4)–Co(1)–O(1)	168.8(1)	O(4)–Co(1)–O(1)	90.4(1)
O(4)–Co(1)–O(3)	88.28(8)		
O(2)–Co(2)–O(2)′	86.4(1)	O(3)–Co(2)–O(2)	90.5(1)
O(3)–Co(2)–O(2)	97.4(1)	O(3)–Co(2)–O(3)′	169.2(1)
O(4)–Co(2)–O(2)	93.67(9)	O(4)–Co(2)–O(2)	170.9(1)
O(4)–Co(2)–O(3)	91.6(1)	O(4)–Co(2)–O(3)	80.5(1)
O(4)–Co(2)–O(4)′	87.6(1)		
O(2)–P(1)–O(1)	106.0(2)	O(3)–P(1)–O(1)	110.2(1)
O(3)–P(1)–O(2)	111.4(1)	O(3)–P(1)–O(3)′	107.6(2)
Co(1)–O(1)–Co(1)′	101.6(1)	P(1)–O(1)–Co(1)	127.6(2)
P(1)–O(1)–Co(1)	130.8(2)	Co(2)–O(2)–Co(2)′	93.6(1)
P(1)–O(2)–Co(2)	126.0(1)	Co(2)–O(3)–Co(1)	107.7(1)
P(1)–O(3)–Co(1)	133.4(1)	P(1)–O(3)–Co(2)	118.3(1)
Co(2)–O(4)–Co(1)	123.3(1)	Co(2)–O(4)–Co(2)′	92.4(1)

[a] H-bond linkage.

A "3-ring" formed of a combination of 4-, 5-, and 6-coordinate centers (Fig. 1) results. Of the two crystallographically distinct cobalt atoms, Co(1) (site symmetry: . . m) is a fivefold coordinated by O atoms in approximately trigonal–pyramidal geometry, with one of the apical positions occupied by an OH group. Co(2) (site symmetry: . . 2) is in a distorted octahedral geometry, with two long (2.264(2) Å) apical Co(2)–O(3) bonds, and four shorter equatorial links, two of which are hydroxide groups in *cis* configuration. The expected high-spin Co^{II}–O bond length, on the basis of ionic-radii sums is

TABLE 6
Atomic Positional and Thermal Parameters for $Zn_2(OH)PO_4$

Atom	x	y	z	U_{eq}[a]
Zn(1)	0.36507(9)	0.36259(8)	1/2	0.0107
Zn(2)	1/2	0	0.2532(1)	0.0152
P(1)	0.2504(2)	0.2392(2)	0	0.0085
O(1)	0.1133(6)	0.1103(5)	0	0.0119
O(2)	0.4164(5)	0.1455(5)	0	0.0102
O(3)	0.2339(4)	0.3468(4)	0.2090(6)	0.0121
O(4)	0.3852(6)	0.1231(5)	1/2	0.0101
H(1)	0.277(2)	0.081(5)	1/2	0.08(4)[b]

[a] U_{eq}(Å^2) = $(U_1U_2U_3)^{1/3}$.
[b] U_{iso}.

TABLE 7
Bond Distances (Å) and Angles (°) for $Zn_2(OH)PO_4$

Zn(1)–O(1)	2.070(4)	Zn(1)–O(1)′	2.024(5)
Zn(1)–O(3) × 2	2.040(3)	Zn(1)–O(4)	2.002(4)
Zn(2)–O(2) × 2	2.052(3)	Zn(2)–O(3) × 2	2.296(3)
Zn(2)–O(4) × 2	2.021(3)		
P(1)–O(1)	1.545(5)	P(1)–O(2)	1.555(5)
P(1)–O(3) × 2	1.542(3)		
O(3) ··· H(1)[a]	2.31(4)	O(4)–H(1)	0.95(1)
O(1)–Zn(1)–O(1)′	78.7(2)	O(3)–Zn(1)–O(1)	96.2(1)
O(3)–Zn(1)–O(1)	121.67(9)	O(3)–Zn(1)–O(1)	96.2(1)
O(3)–Zn(1)–O(3)	116.6(2)	O(4)–Zn(1)–O(1)	170.5(2)
O(4)–Zn(1)–O(1)	91.7(2)	O(4)–Zn(1)–O(3)	88.8(1)
O(2)–Zn(2)–O(2)′	85.2(2)	O(3)–Zn(2)–O(2)	91.0(1)
O(3)–Zn(2)–O(2)	97.3(1)	O(3)–Zn(2)–O(3)′	168.7(2)
O(4)–Zn(2)–O(2)	94.9(1)	O(4)–Zn(2)–O(2)	171.1(2)
O(4)–Zn(2)–O(3)	91.5(1)	O(4)–Zn(2)–O(3)	80.2(1)
O(4)–Zn(2)–O(4)′	86.5(2)		
O(2)–P(1)–O(1)	105.9(2)	O(3)–P(1)–O(1)	110.0(2)
O(3)–P(1)–O(2)	111.6(2)	O(3)–P(1)–O(3)′	107.9(3)
Zn(1)–O(1)–Zn(1)′	101.3(2)	P(1)–O(1)–Zn(1)	129.2(3)
P(1)–O(1)–Zn(1)	129.6(3)	Zn(2)–O(2)–Zn(2)′	94.8(2)
P(1)–O(2)–Zn(2)	125.6(1)	Zn(2)–O(3)–Zn(1)	108.1(1)
P(1)–O(3)–Zn(1)	132.9(2)	P(1)–O(3)–Zn(2)	118.3(2)
Zn(2)–O(4)–Zn(1)	122.9(1)	Zn(2)–O(4)–Zn(2)′	93.5(2)

[a] H-bond linkage.

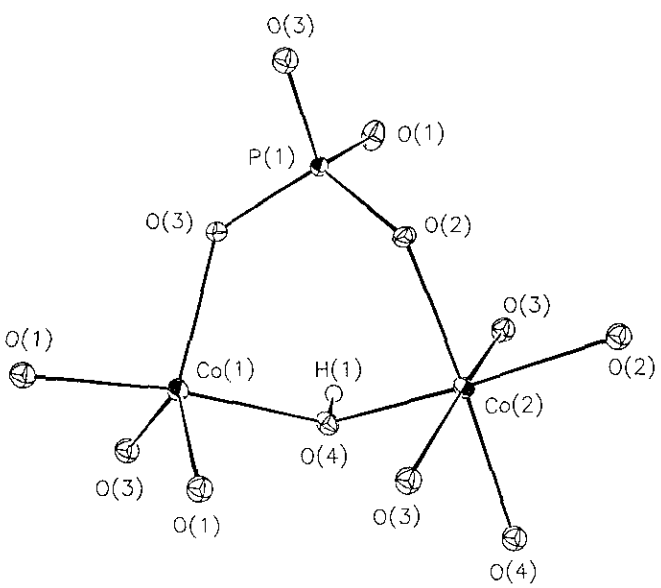

FIG. 1. ORTEP view of the polyhedral building units of $Co_2(OH)PO_4$, showing the "3-ring" of $Co(OH)_2O_4$, $Co(OH)O_4$, and PO_4 units; 50% thermal ellipsoids (arbitrary proton radius).

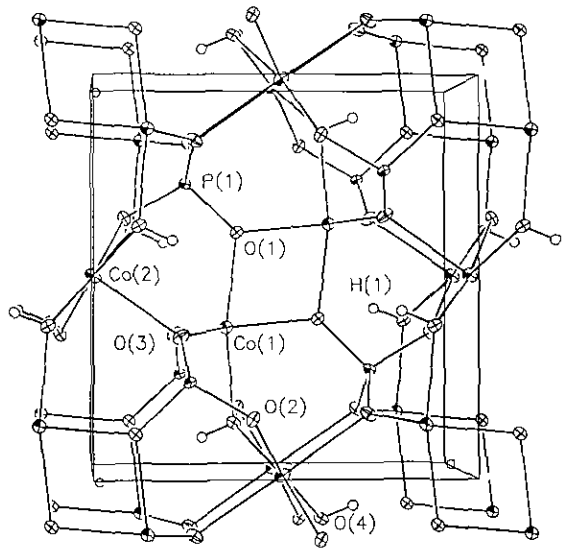

FIG. 2. ORTEP view of unit-cell packing of $Co_2(OH)PO_4$, viewed down the c unit-cell direction, with selected atoms labeled (50% thermal ellipsoids). $Zn_2(OH)PO_4$ is isostructural with $Co_2(OH)PO_4$.

2.11 Å (22). The ZnO_6 octahedron in $Zn_2(OH)PO_4$ shows a similar axial distortion, with a Zn–O(3) bond length of 2.296(3) Å (ionic radii sum = 2.10 Å). P(1) (site symmetry: . . m) shows typical, regular, tetrahedral phosphate coordination. Of the four distinct oxygen atoms, O(1), O(2) and O(3) each bond to two cobalt atoms and one phosphorus atom, while O(4) is linked to three distinct cobalt atoms, as well as to a proton.

The structure is built up from edge-sharing strings of $Co(2)O_6$ octahedra, which propagate in the c-direction, the bridging oxygen atoms being alternate pairs of O(2)s and O(4)s, the latter being the hydroxide oxygen atom. These Co(2) chains are crosslinked (via oxygen-atom O(4) bridges) by pairs of Co(1) atoms (with trigonal pyramidal coordination) which themselves share an edge via two O(1) atoms. Finally, the phosphate group partakes in four distinct P–O–[2 × Co] bonds [each bond links to two Co(1) and/or Co(2)], resulting in a condensed structure without any identifiable channels or pores. The topological description of $Zn_2(OH)PO_4$ is identical to that of $Co_2(OH)PO_4$, with Zn(1) and Zn(2) substituting for Co(1) and Co(2), respectively. The two zinc-atom environments in the $Zn_2(OH)PO_4$ structure are illustrated in Figs. 3 and 4.

Average bond distances for the Co and P atoms in $Co_2(OH)PO_4$ are as follows: d_{av}[Co(1)–O] = 2.033(3) Å, d_{av}[Co(2)—O] = 2.120(1) Å, and d_{av}[P(1)–O] = 1.542(2) Å. Bond valence sum (BVS) values, calculated according to the Brese–O'Keefe formalism (23), are also characteristic: BVS[Co(1)] = 2.00, BVS[Co(2)] = 1.96, and BVS[P(1)] = 4.73. The three tribridging oxygen

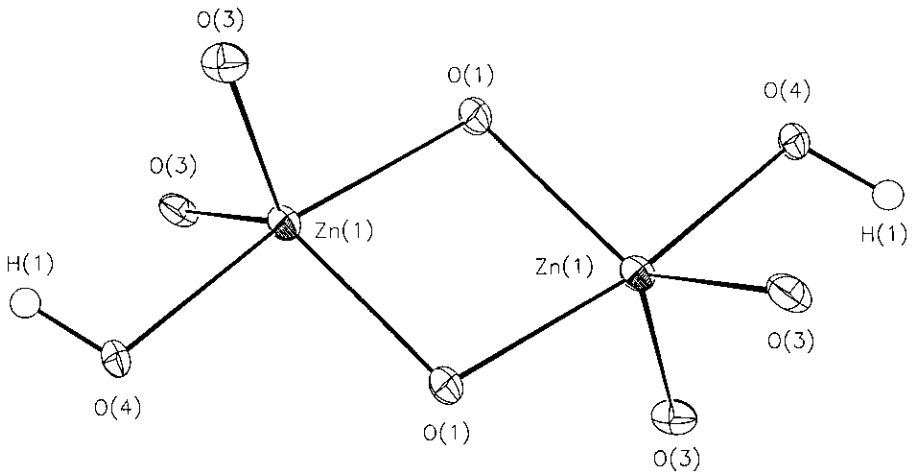

FIG. 3. Detail of the Zn(1) atom environment in $Zn_2(OH)PO_4$, showing the edge-sharing pair of ZnO_5 groups; 50% thermal ellipses (arbitrary radius for the proton).

atoms (to 2 Co + 1 P) have BVS values close to 2.00 (BVS[O(1)] = 1.97, BVS[O(2)] = 1.89, and BVS[O(3)] = 2.00), while the remaining oxygen atom, O(4), which links the 5- and 6-coordinate Co atom centers, has a BVS of only 1.22 if the proton contribution is neglected. This proton, H(1), is involved in a very long ($d \sim 2.3$ Å) H-bond to O(3).

Typical average bond distances also result for the zinc and phosphorus atomic coordinations in $Zn_2(OH)PO_4$: d_{av}[Zn(1)–O] = 2.035(2) Å, d_{av}[Zn(2)–O] = 2.123(2) Å and d_{av}[P(1)–O] = 1.546(3) Å. BVS values for $Zn_2(OH)PO_4$ are typical: BVS[Zn(1)] = 1.98, BVS[Zn(2)] = 1.96, and BVS[P(1)] = 4.91. The three tribridging oxygen atoms all have BVS values of ca. 2.00 (BVS = 1.95, 2.00, and 2.02 for O(1), O(2), and O(3) respectively), while O(4) has a BVS of only 1.26 if the proton contribution is neglected. As in $Co_2(OH)PO_4$, this proton, H(1), is involved in a long ($d \sim 2.3$ Å) hydrogen-bond link to O(3). Hawthorne (2) suggested that the proton in $Zn_2(OH)AsO_4$ makes a similar H bond link to O(3), based on IR spectra and BVS values.

PHYSICAL PROPERTIES OF $Co_2(OH)PO_4$ AND $Zn_2(OH)PO_4$

Thermogravimetric analysis of $Co_2(OH)PO_4$ indicated an initial 0.4% weight loss, and a further 3.8% weight loss at ~600°C. We attribute the initial weight loss to surface effects, and the 600°C weight decrease to loss of water from the sample (calc = 3.9%). The powder X-ray diffraction pattern of the purple, post-TGA residue showed the presence of CoO and $Co_3(PO_4)_2$. TGA for $Zn_2(OH)PO_4$ showed a weight loss of 3.85% by ~600°C (weight loss predicted for total water loss: 3.71%), and powder X-ray diffraction indicated that the post-TGA residue contained ZnO and $Zn_3(PO_4)_2$. The decomposition process for both materials may be written as

$$2M_2(OH)PO_4 \xrightarrow{\Delta} MO + M_3(PO_4)_2 + H_2O.$$

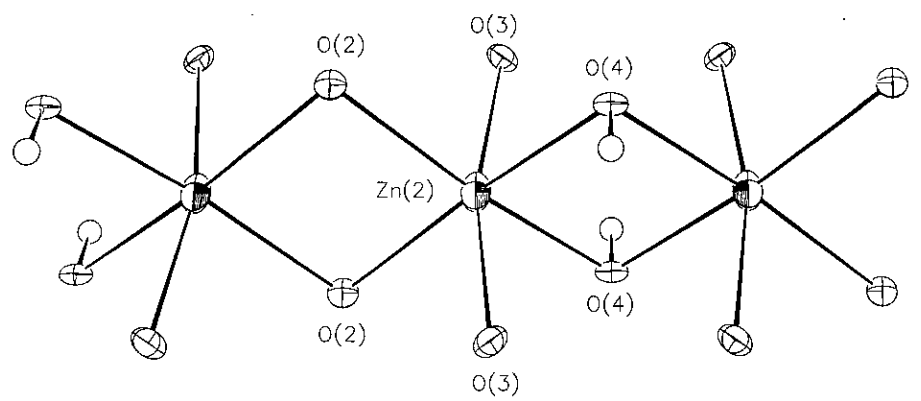

FIG. 4. Detail of the Zn(2) atom environment in $Zn_2(OH)PO_4$, showing the infinite, edge-sharing ZnO_6 octahedral chain, which propagates in the c-direction; 50% thermal ellipses; arbitrary radius for the proton. Note the alternate edge linkages of pairs of O(2) and O(4) atoms.

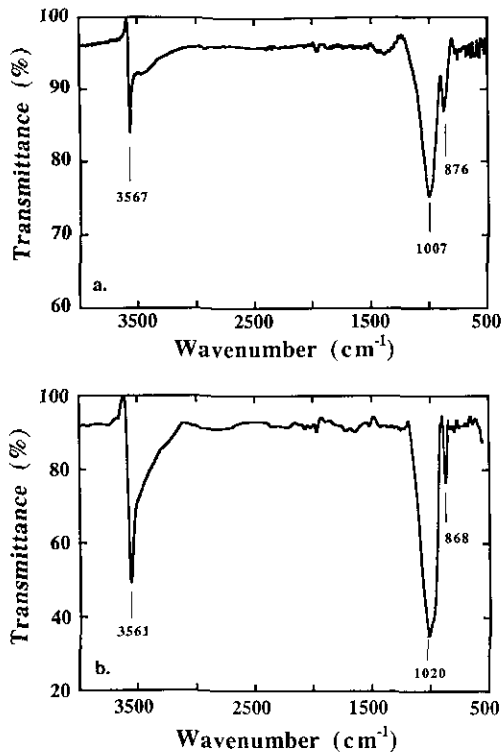

FIG. 5. (a) IR spectrum of $Co_2(OH)PO_4$; (b) IR spectrum of $Zn_2(OH)PO_4$.

The IR spectrum of $Co_2(OH)PO_4$ (Fig. 5) shows three distinct features. The sharp band at ~3567 cm^{-1} is attributable to a bridging–OH group, while the phosphate group contributes to the broad band at 1200–900 cm^{-1} (asymmetric stretch ν_3) and a weak, narrow band at ~876 cm^{-1} (symmetric stretch ν_1) (24). The same three bands are visible in the IR spectrum of $Zn_2(OH)PO_4$ (Fig. 5).

DISCUSSION

For the first time $Co_2(OH)PO_4$ and $Zn_2(OH)PO_4$ were prepared and structurally characterized. Their physical properties are consistent with their crystal chemistry. Both phases are $M_2(OH)XO_4$ adamite isomorphs, further increasing the variety of this structure type. Unit cell data for the well-characterized adamite-type phases are listed in Table 8. While it is common for simple inorganic phases to show isomorphism, an interesting structural feature of all these materials is the distorted MO_6 octahedron, which shows a typical difference in axial versus equatorial M–O bond lengths of ~0.25 Å. This distortion cannot be correlated with any electronic behavior of the M^{2+} or M^{3+} cation, since all the adamite-type phases show this structural effect, regardless of the metal d-electron configuration, nor do bond-valence-sum calculations show any particular anomalies for the oxygen atom environments (*vide supra*). Hawthorne (2) rationalized this octahedral distortion in adamite-type materials in terms of the requirement of the MO_6 octahedron to "stretch" to allow the adjacent MO_5 unit to incorporate a cation with ionic radius ~0.7 Å. In any event, the overall stability of the adamite structure is sufficient to incorporate this axially distorted octahedral group for a number of divalent cations.

Another previously characterized phase of stoichiometry $Zn_2(OH)PO_4$, the mineral tarbuttite (25), crystallizes in a different triclinic structure than the adamite-type phases. This triclinic structure was also found for a second natural form of $Zn_2(OH)AsO_4$ (paradamite) (26). The tarbuttite structure contains two different trigonal–bipyramidal ZnO_5 groups, and a tetrahedral PO_4 moiety. The polyhedral packing, involving edge-sharing of the ZnO_5 groups, and corner-sharing between the ZnO_5 and PO_4 units (25) is quite similar to the $ZnO_6/ZnO_5/PO_4$ situation in adamite-type $Zn_2(OH)PO_4$. As was also noted by Hawthorne (2), for the case of adamite $Zn_2(OH)AsO_4$ (ρ = 4.44 g/cm^3) versus paradamite $Zn_2(OH)AsO_4$ (ρ = 4.58 g/cm^3), tarbuttite-type $Zn_2(OH)AsO_4$ (ρ = 4.22 g/cm^3) is slightly denser than adamite-type $Zn_2(OH)PO_4$ (ρ = 4.00 g/cm^3). Thus, tarbuttite may be the stable polymorph of $Zn_2(OH)PO_4$ when prepared at higher pressures. Synthetic tarbuttite has been hydrothermally prepared from a starting mixture of Li_2O, ZnO, P_2O_5, and H_2O (27), but unfortunately, full details of the preparation conditions were not provided. We note that lithium was apparently required in the synthesis, but not incorporated into the tarbuttite-type $Zn_2(OH)PO_4$ product. Under very mild conditions, the ABW-type phase $LiZnPO_4 \cdot H_2O$ and the unusual "semicondensed" $LiZnPO_4$ are also accessible from the $Li_2O/ZnO/P_2O_5/H_2O$ system (28).

Adamite-type $Co_2(OH)PO_4$ complements a number of other known cobalt–phosphate hydrates/hydroxides. A search of the Inorganic Crystal Structure Database (ICSD) (29) indicated 12 other Co/P/O/H phases which have been structurally characterized. For the Zn/P/O/H combination, 26 "hits" were recorded by ICSD. Thus, it is perhaps surprising that $Co_2(OH)PO_4$ and $Zn_2(OH)PO_4$ have not been discovered in nature, or synthesized previously, in these well-studied regions of phase space. However, the presence of *organic* reagents, which are not incorporated into the adamite-type products, in both the syntheses described here is notable. Such "structure-directing" effects are well known in molecular sieve synthesis, and may lead to novel aluminophosphates (30) and zincophosphates (31), in which the organic group is included in the final crystalline product. Here, the organic reagent is required for $Co_2(OH)PO_4$ and $Zn_2(OH)PO_4$ formation, but is not incorporated into the *condensed* structure of the adamite-type products. Its role is certainly important in adjusting the pH to the narrow range required for formation of the adamite-type phases. However, the

TABLE 8
Summary of Adamite-Type Unit Cells

Formula	a(Å)	b(Å)	c(Å)	V(Å^3)	Ref.
Al_2OSiO_4	7.7942(2)	7.8985(2)	5.559(2)	342.23	(7)
$Al_{1.14}Mn_{0.86}OSiO_4$	7.959(2)	8.047(2)	5.616(1)	359.68	(8)
$Fe_{1.14}Al_{0.85}OGeO_4$	8.1006(1)	8.2259(1)	5.8259(1)	388.21	(9)
$Co_2(OH)PO_4$	8.042(3)	8.369(3)	5.940(2)	399.80	This work
$Zn_2(OH)PO_4$	8.103(2)	8.3292(9)	5.9659(8)	402.65	This work
$Cu_2(OH)PO_4$	8.110	8.470	5.920	406.66	(32)
$Co_2(OH)AsO_4$	8.248(6)	8.551(9)	6.036(5)	425.71	(6)
$Zn_2(OH)AsO_4$	8.304(2)	8.530(2)	6.047(1)	428.33	(2)
$(Cu, Zn)_2(OH)AsO_4$	8.5(2)	8.52(2)	5.99(1)	433.80	(33)
$Mn_2(OH)AsO_4$	8.57(1)	8.77(1)	6.27(1)	471.25	(3)

Note. All phases are orthorhombic, with unit cells transformed, if necessary, to conform with the standard *Pnnm* space-group setting; cell parameter esd's are given where known.

large size of the organic cation prevents its inclusion in the adamite-type products under the reaction conditions used here. Conversely, the use of ammonium cations to control pH results in the ammonium-containing phases noted in the experimental section. We are continuing our exploratory synthesis efforts in this area—*open framework* organo cobaltophoshate phases may be accessible under appropriate experimental conditions.

ACKNOWLEDGMENTS

We thank Ivan Bernal (Houston) for access to diffractometer facilities. This work is partially funded by the National Science Foundation (DMR-9214804) and the Welch Foundation.

REFERENCES

1. W. E. Richmond, *Am. Mineral.* **25,** 441 (1940).
2. F. C. Hawthorne, *Can. Mineral.* **14,** 143 (1976).
3. P. B. Moore and J. R. Smythe, *Am. Mineral.* **53,** 1841 (1968).
4. A. Cordsen, *Can. Mineral.* **16,** 153 (1978).
5. H. Heritsch, *Z. Kristallogr.* **99,** 466 (1938).
6. H. Riffel, F. Zettler, and H. Hess, *Neues Jahrb. Mineral. Montash.* 514 (1975).
7. C. W. Burnham and M. J. Buerger, *Z. Kristallogr.* **115,** 269 (1961).
8. Z. Weiss, S. W. Bailey, and M. Rieder, *Am. Mineral.* **66,** 561 (1981).
9. R. X. Fischer and H. Schneider, *Z. Kristallogr.* **201,** 19 (1992).
10. P. Lightfoot and A. K. Cheetham, *Acta Crystallogr. C* **44,** 1331 (1988).
11. A. Durif and M. T. Averbuch Pouchot, *Bull. Soc. Fr. Mineral. Cristallogr.* **91,** 495 (1968).
12. A. Whitaker, *Acta Crystallogr. B* **31,** 2026 (1975).
13. M. T. Averbuch Pouchot, *Mater. Res. Bull.* **3,** 719 (1968).
14. K. Yvon, W. Jeitscho, and E. Parthe, *J. Appl. Crystallogr.* **10,** 73 (1977).
15. P. D. Baird, "RC85 User Guide." Chemical Crystallography Laboratory, Oxford University, Oxford, UK, 1985.
16. M. S. Lehmann and F. K. Larsen, *Acta Crystallogr. A* **30,** 580 (1974).
17. G. M. Sheldrick, "Shelxs-86 User Guide." Crystallography Department, University of Göttingen, Germany, 1986.
18. A. C. Larson, *Acta Crystallogr.* **23,** 664 (1967).
19. "International Tables for X-Ray Crystallography," Vol. IV. Kynoch Press, Birmingham 1974.
20. D. J. Watkin, J. R. Carruthers and P. W. Betteridge, "CRYSTALS User Guide." Chemical Crystallography Laboratory, Oxford University, UK, 1985.
21. J. R. Carruthers and D. J. Watkin, *Acta Crystallogr. A* **35,** 698 (1979).
22. R. D. Shannon, *Acta Crystallogr. A* **32,** 751 (1976).
23. N. Brese and M. O'Keefe, *Acta Crystallogr. B* **47,** 192 (1991).
24. K. Nakamoto, "Infrared and Raman Spectra of Inorganic and Coordination Compounds," 9th ed., Wiley–Interscience, New York, 1986.
25. G. Cocco, L. Fanfani, and P. F. Zanazzi, *Z. Kristallogr.* **123,** 321 (1966).
26. T. Kato and Y. Miura, *Miner. J. Jpn.* **8,** 320 (1977).
27. E. A. Genkina, B. A. Maksimov, and O. K. Mel'nikov, *Dokl. Akad. Nauk SSSR* **282,** 314 (1985); [Transl: (*Sov. Phys. Dokl.* **30,** 329 (1985)]
28. W. T. A. Harrison, T. E. Gier, J. M. Nicol, and G. D. Stucky, *J. Solid State Chem.*, (1995) in press.
29. "Inorganic Crystal Structure Database." The University of Bonn, Germany, November 1993.
30. E. M. Flanigen, B. M. Lok, R. L. Patton, and S. T. Wilson, *in* "New Developments in Zeolite Science and Technology." Elsevier, Amsterdam, 1986.
31. W. T. A. Harrison, T. E. Martin, T. E. Gier, and G. D. Stucky, *J. Mater. Chem.* **2,** 175 (1992).
32. E. M. Walitzi, *Tscher. Mineral. Petrogr. Mitt.* **8,** 614 (1963).
33. K. Toman, *Acta Crystallogr. B* **34,** 715 (1978).